IEEE Access
Multidisciplinary ⋮ Rapid Review ⋮ Open Access Journal

Received December 18, 2019, accepted January 9, 2020, date of publication February 4, 2020, date of current version February 11, 2020.

Digital Object Identifier 10.1109/ACCESS.2020.2969723

Design, Fabrication and Test of a Low Range Capacitive Accelerometer With Anti-Overload Characteristics

YUNBO SHI[1,2], YANLIN WANG[1,2], HENGZHEN FENG[3], RUI ZHAO[1,2], HUILIANG CAO[1,2], (Member, IEEE), AND JUN LIU[1,2]

[1]School of Instrument and Electronics, North University of China, Taiyuan 030051, China
[2]Science and Technology on Electronic Test and Measurement Laboratory, North University of China, Taiyuan 030051, China
[3]School of Mechatronical Engineering, Beijing Institute of Technology, Beijing 100081, China

Corresponding authors: Huiliang Cao (caohuiliang1986@126.com) and Jun Liu (liuj@nuc.edu.cn)

This work was supported in part by the National Natural Science Foundation of China under Grant 51705477, Grant 61703098, and Grant 61603353, in part by the Pre-Research Field Foundation of Equipment Development Department of China under Grant 61405170104, in part by the Top Young Academic Leaders of Higher Learning Institutions of Shanxi, Fund Program for the Scientific Activities of Selected Returned Overseas Professionals in Shanxi Province, Shanxi Province Science Foundation for Youths under Grant 201801D221195, in part by the Young Academic Leaders of North University of China under Grant QX201809, in part by the Weapons and Equipment Joint Fund under Grant 6141B021304, and in part by the Fund for Shanxi "1331 Project" Key Subjects Construction.

ABSTRACT Capacitive accelerometers have been widely used in the fields of mobile phones, automobiles, seismic monitoring and others because of its high sensitivity, good repeatability and high precision. This type of accelerometer usually has a low range. The sensitive structure of the sensor is too vulnerable to damage in high impact environments, so it basically has no ability to detect smaller signals after a relatively high acceleration. This paper presents a capacitive accelerometer which employs a four-terminal fixed structure. Acceleration is outputted by a differential capacitance formed between the mass and the upper and lower glass plates. With consideration of better anti-overload capability and small signal detection capability, structure optimization and anti-overload protection such as chamfer and protection measures have been carried out. According to the simulation results of the optimized structure by finite element analysis software, it has a maximum stress of 62 Mpa when a 20,000g shock is load, the maximum displacement within effective range (100g) is 13.7 μm, and it also has a first-order frequency response of 7.477 kHz. And then, the process flow is designed and the device is fabricated. Static capacitance test and flip test are utilized to verify its static performance. The anti-overload capability of the device is tested and verified by Marshall Hammer impact experiments.

INDEX TERMS Microelectromechanical systems, capacitive sensors, sandwich structure, microfabrication, anti-overload.

I. INTRODUCTION

Capacitive micromechanical accelerometer is one of the important directions in the field of MEMS accelerometer with its high resolution and high stability. It is widely used in military fields such as space acceleration detection and guided weapons, it also plays an important role in civilian fields such as automotive safety systems and medical services [1]–[3]. Various structures of capacitive accelerometers had been developed, such as the comb-tooth, torsion, cantilever and "sandwich" structures [4]. ION company developed a capacitive accelerometer for seismic detection with a temperature range is −40°C to 50°C and an excellent low frequency performance, whose structure composed of four independent single crystal lithographic silicon wafers. A comb-type capacitive accelerometer based on TSV packaging technology was developed by The Middle East Technical University of Turkey, which working frequency was 9.45kHz and sensitivity is 1.6pF/g. Due to its high sensitivity, it was widely used in geological surveys, meanwhile it

The associate editor coordinating the review of this manuscript and approving it for publication was wuliang Yin.

was easy to fail in high impact environments [5]. A dual-axis capacitive accelerometer used multi-layer gold plating process was designed in [6], its single gold proof mass worked as a dual-axis sensing electrode and therefore it could detect a broad range of acceleration with sub-1G resolution on a single sensor chip. In [7], a capacitive accelerometer with double-sided symmetrical U-shaped beams was proposed, the sensitivity was up to 15pF/g and non-linearity was 0.6% in a range of 0g to 1g. A micro-mechanical differential capacitive accelerometer based on low-temperature co-fired ceramic(LTCC) was developed in [8], which had four L-shaped cantilever beams embedded in LTCC multilayer substrate and a capacitance detection chip on the surface of upper plate. It had an excellent linearity in a small impact environment and a sensitivity of 30.3mV/g. The test results showed that it had a certain ability of anti-overload, but the cost and the difficulty of processing of the material restricted its applicability. A MEMS capacitive accelerometer with fully symmetrical double-sided H-shaped beam structure was presented in [9], which fabricated from a single double-device-layer SOI wafer. The high controllable dimension H-shaped beams suspend the mass with a thickness of 560μm. The quality factor and the resonant frequency were 106 and 2.24 kHz. Within the measurement range of 1g, it had a sensitivity of 0.24V/g and a nonlinearity of 0.29%. In [10], a novel capacitive Z-axis (out of plane) accelerometer was proposed, it contained differential capacitive sensing electrodes with a gap closing design on an SOI wafer. The electrical connection between the device and operating silicon layers of the SOI wafer was available by means of the metal vias. The test results indicated that it had a sensitivity of 196.3mV/G(42.5fF/G) and a maximum nonlinearity of 2% over the range of 0.1–1G. A highly symmetric sandwich accelerometer using a double-device-layer silicon-on-insulator (D-SOI) wafer was presented in [11], with eight L-shaped symmetric beams suspended the proof mass of though-wafer-thickness. The accelerometer was insensitive to the lateral acceleration and rotation disturbance since the sensing mode (first vibration mode) was decoupled from other variation modes that followed. It had a high sensitivity of 55pF/g.

MEMS capacitive accelerometer has been widely developed with its high reliability and precision, but it was hard to apply in dynamic testing, especially in high impact test environment. This is mainly due to the contradiction between sensitivity and anti-overload. The working environment of anti-overload accelerometer is generally harsh. It is important that the sensor has a sturdy structure to avoid damage in high impact environments, however it is incompatible with the purpose of high-precision. Therefore, less research has been done on accelerometer that can meet the characteristics of anti-overload and high sensitivity in the low range. In this paper, a capacitive accelerometer is proposed, together with its performance testing. Four beams and central-island mass style has been adopted for the accelerometer, the differential capacitor which is formed of the electrodes between the sandwich structure transforms the acceleration signals. The reliability of the structure is intensified by adding the protection measures and reducing the excessive stress concentration in the root part of the beams. Accurate measurement can be achieved within the safe displacement range of the mass. The rest of the paper is organized as follows: Section II designs the accelerometer structure, Section III investigates the manufacture process of the capacitive accelerometer structure, Section IV tests the performance of the accelerometer, and Section V concludes.

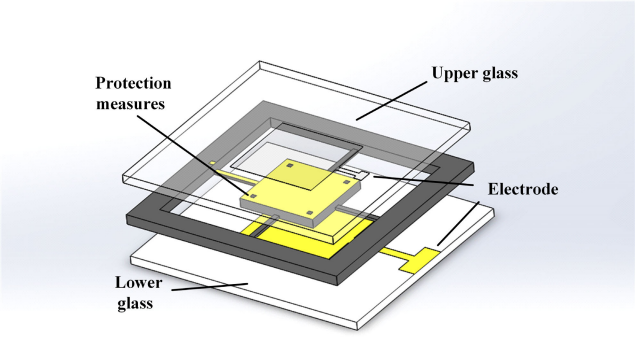

FIGURE 1. Sandwich structure model.

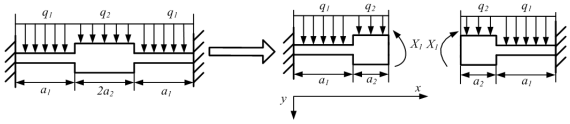

FIGURE 2. Structural model.

II. STRUCTURAL DESIGN ANALYSIS

A. STRUCTURAL MODEL DESIGN

The capacitive accelerometer adopts an anodic bonding mode with a glass-silicon-glass sandwich structure. Silicon is used to design four cantilever beams, and then the signals can be detected accurately. The structure model is shown in Fig. 1. According to the force characteristics, the cantilever beams can be simplified as shown in Fig. 2. In the model, the length, width and thickness of the beam are a_1, b_1 and h_1, respectively. The length, width and thickness of the mass are $2a_2$, b_2 and h_2. When the structure is struck along the Y axis, the loads that the cantilever beams and mass receive are q_1 and q_2 [12].

The excess restraint moment is X_1. According to the canonical equation, X_1 can be expressed as:

$$X_1 = -\frac{\Delta_{1F}}{\delta_{11}} = \frac{-\frac{q_2 a_2^3}{6EI_2} - \frac{q_2 a_1 a_2^2}{2EI_1} - \frac{q_2 a_1^2 a_2}{2EI_1} - \frac{q_1 a_1^3}{6EI_1}}{\frac{a_1}{EI_1} + \frac{a_2}{EI_2}} \quad (1)$$

where E is the Young's modulus of the silicon, I_1 and I_2 is inertia moments of beam and mass respectively.

The formula is resolved as follows:

$$X_1 = -\frac{I_1 q_2 a_2^3 + 3I_2 q_2 a_1 a_2^2 + 3I_2 q_2 a_1^2 a_2 + I_2 q_1 a_1^3}{6(I_1 a_2 + I_2 a_1)} \quad (2)$$

The moment equation for any cross-section of the beam is:

$$M(x) = \begin{cases} -q_2 a_2 \left(a_1 + \frac{a_2}{2} - x\right) - \frac{q_1 (a_1 - x)^2}{2} + X_1 \\ \qquad 0 \le x \le a_1 \\ -\frac{q_2 (a_1 + a_2 - x)^2}{2} + X_1 \\ \qquad a_1 < x \le (a_1 + a_2) \end{cases} \quad (3)$$

Therefore, the differential equation of the deflection of the structure is:

$$EIy''(x) = M(x) = \begin{cases} -q_2 a_2 (a_1 + \frac{a_2}{2} - x) - \frac{q_1 (a_1 - x)^2}{2} + X_1 \\ \qquad 0 \le x \le a_1 \\ -\frac{q_2 (a_1 + a_2 - x)^2}{2} + X_1 \\ \qquad a_1 < x \le (a_1 + a_2) \end{cases} \quad (4)$$

The boundary conditions are:

$$\begin{cases} y'(a_1^-) = y'(a_1^+) = 0 \\ y(a_1^-) = y(a_1^+) = 0 \\ y(0) = 0 \\ y'(0) = 0 \end{cases} \quad (5)$$

The structure mechanical sensitivity can be got that:

$$z(x) = \frac{1}{EI} \begin{cases} -\frac{1}{24} q_1 (a_1 - x)^4 - \frac{q_2 a_2}{6} \left(a_1 + \frac{a_2}{2} + x\right)^3 + \frac{X_1}{2} x^2 \\ + \frac{q_1 a_1^4}{24} + \left[-\frac{q_2 q_3}{2} \left(a_1 + \frac{a_2}{2}\right) - \frac{q_1 a_1^3}{6} \right] x \\ + \frac{q_2 a_2}{6} \left(a_1 + \frac{a_2}{2}\right)^3, 0 < x \le a_1 \\ -\frac{1}{24} q_2 (a_1 + a_2 - x)^4 \\ + \left[\frac{1}{24} q 2 a_2^3 - \frac{q_2 a_2}{2} \left(a_1 + \frac{a_2}{2}\right)^3 - \frac{q_1 a_1^3}{6} \right] x + \frac{X_1}{2} x^2 \\ + \frac{q_1 a_1^4}{24} + \frac{q_2 a_2}{6} \left(a_1 + \frac{a_2}{2}\right)^3 + \frac{q_1 a_1 a_2^3}{2}, a_1 \le x \le a_1 + a2 \end{cases} \quad (6)$$

According to [13], the first order natural frequency of the structure is:

$$\omega_n^2 = \frac{\int_0^{a_1} EI\,[z(x)\,"]^2 dx}{\frac{1}{2} m\,[z(a_1)]^2} = \frac{2Eb_1 h_1^3}{m a_1^3} \quad (7)$$

Combining formulas "(2)" and "(3)", the polynomial equation is solved in MATLAB, and the deflection y(x) of the structure can be calculated. After the analysis of the structure, it can be found that a shorter, wider and thicker cantilever improves the resonance frequency and has a small influence on the sensitivity [14], [15]. Then, the width and length parameters of the beam are optimized by utilizing a MATLAB simulation (the resonance frequency of the structure can be adjusted later by verifying the thickness value h_1), and the deflection, stress, resonance frequency and mechanical sensitivity are analyzed; the results are shown in Fig. 3 and Fig. 4. It can be seen from the figures that a larger a1 and a smaller b1 decrease the stress and increase the structure sensitivity and resonance frequency [16].

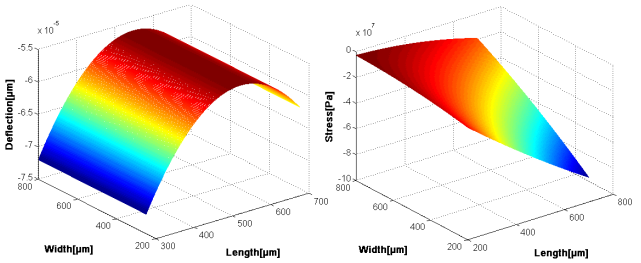

FIGURE 3. Relationship between the deflection(left), stress(right), beam length and beam width.

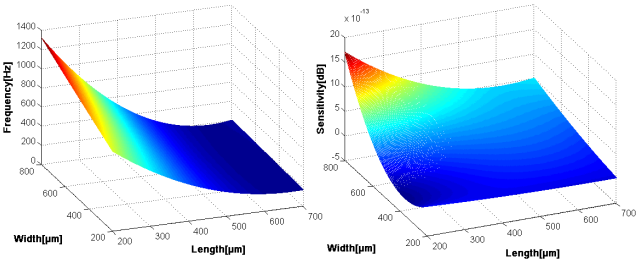

FIGURE 4. Relationship between the frequency(left), sensitivity(right), beam length and beam width.

TABLE 1. Structural parameters of the silicon sensor.

	Mass	Beam	Frame
Length (μm)	1,600	1,200	5,200
Width (μm)	1600	120	600
Thickness (μm)	270	30	300

After considering the sensor performance and manufacturing method, the structural parameters of the structure are optimized and shown in Table 1:

B. STATIC ANALYSIS OF THE SENSOR

Static analysis is used to calculate the strain and displacement responses of structures under stable stress and constant loads [17]. The equivalent stress distribution of the sensor structure is shown in Fig. 5(a), and the equivalent displacement distribution is shown in Fig. 5 (b), after an acceleration impact signal of 100g is applied in the sensitive direction of the accelerometer.

After applying an acceleration shock signal of 100g in the sensitive direction Z of the acceleration sensor, the equivalent stress distribution of the sensor structure is shown in Fig. 4(a), and the equivalent displacement distribution is shown in Fig. 4(b).

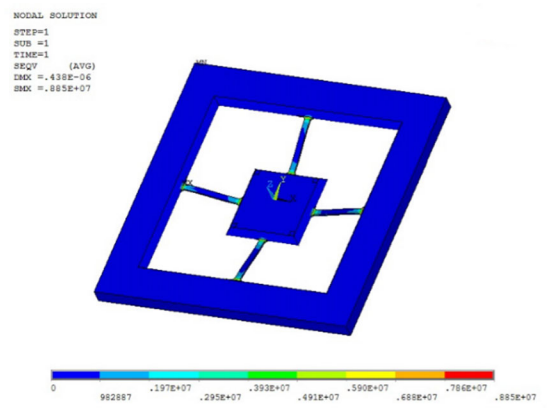

(a) Equivalent stress distribution diagram under a 100g overload

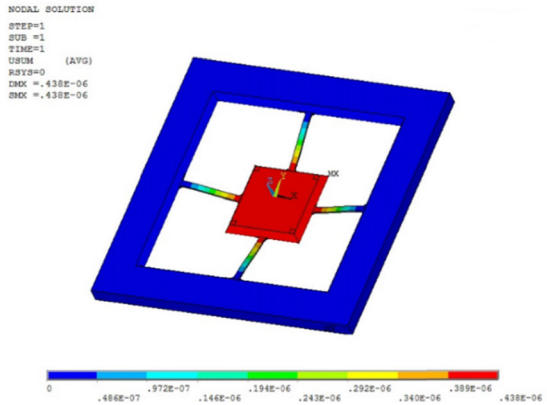

(b) Equivalent displacement distribution diagram under a 100g overload

FIGURE 5. Static simulation of the sensor range.

TABLE 2. Maximum stress, equivalent displacement, capacitance change under different impact conditions.

	20g	50g	80g	100g
Maximum stress (MPa)	6.05	15.15	24.24	30.3
Equivalent displacement (μm)	3.00	7.50	12.00	15.00
Capacitance change (pF)	0.555	1.379	2.207	3.02

According to Fig. 4, the maximum displacement of the mass is 13.7 μm under the 100 g impact. At this moment, the protection is fitted with a glass plate, the equivalent stress of the cantilever beam is 30.3 MPa, and the value is smaller than the allowable stress in silicon (80∼120 MPa).

The variable capacitance is as follows:

$$\Delta C' \approx C_1 - C_2 = (C_0 + \Delta C) - (C_0 - \Delta C) = 2\Delta C \quad (8)$$

Then $\Delta C = 3.02$pF. The sensitivity is calculated with the formula: $\Delta C/a = 3.02 \times 10^{-2}$pF. The maximum stress, the equivalent displacement and the capacitance change linearly with each other under impacts of 20g, 50g, 80g, 100g, and the data are shown in Table 2.

C. HIGH-OVERLOAD ANALYSIS

In addition, a static simulation of the sensor in an overload environment of 20,000g is carried out by considering the working mode of the sensor. At 100g, the mass and the glass substrate are fitted; under the high-overload environment, the shock stress received by the accelerometer is mainly absorbed by the cantilever beams. The maximum stress of the sensor is shown in Fig. 6.

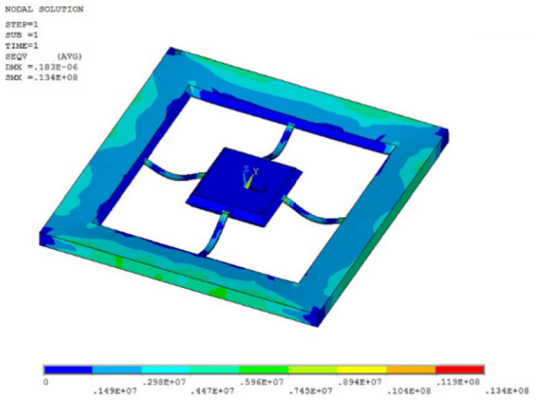

FIGURE 6. Equivalent stress distribution diagram under a high overload.

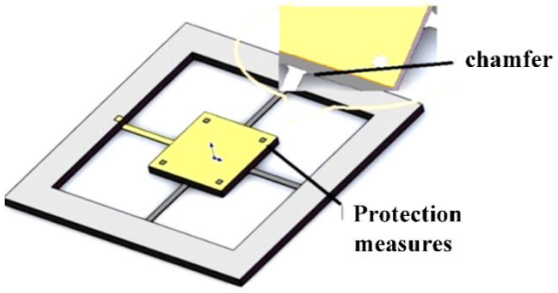

FIGURE 7. Anti-high-overload measures.

The maximum stress is 12.8 MPa, which exceeds the allowable stress in silicon. At the same time, under the high-overload environment, the displacement of the mass is large, and the cantilever beams will break and fail. To ensure the stability of the accelerometer under high-impact conditions, chamfers at both ends of the cantilever beam are introduced to improve the anti-overload characteristics of the sensor. The chamfers are shown in Fig. 7.

By analyzing the influence of different sizes of fillets on the stress dispersion, the best anti-overload performance of the sensor is obtained when the chamfer size is 55 μm. The maximum stress cloud in a high-overload environment is shown in Fig. 8.

Mechanical analysis of the sensor with a chamfer structure under an impact of 20,000 g is carried out:

(1) The mass experiences an impact of 100g, the maximum displacement is 13.7 μm, and the stress at the root of the beam is 30.3 MPa; at this time, the mass block is attached to the glass substrate;

(2) When the impact signal exceeds the range, the mass block is attached to the glass substrate, and the residual impact signal is mainly borne by the cantilever beam. The maximum stress of the sensor is 62 MPa, and the maximum

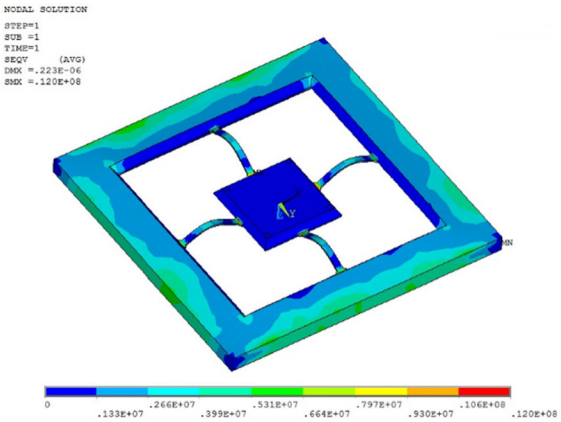

FIGURE 8. Equivalent stress distribution of a chamfer structure under a 20,000 g overload.

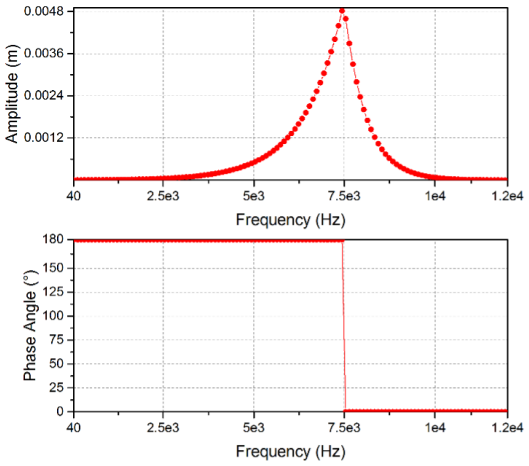

FIGURE 9. Frequency response (magnitude and phase).

TABLE 3. Vibration frequency of each order.

Modal	1	2	3	4	5	6
Frequency (kHz)	7.477	18.066	18.453	41.976	104.12	104.13

displacement is 0.223 μm, which satisfies the allowable stress in the silicon-based material.

D. HARMONIC RESPONSE ANALYSIS

Harmonic response analysis is based on modal analysis, which is mainly used to determine the frequency response characteristics of the accelerometer sensor structure, that is, the natural frequencies and mode shapes of the sensitive structures of the accelerometer.

In this paper, the frequency response of the sensor under 100 g is obtained by the harmonic response. As shown in Fig. 8, combined with modal analysis, the frequency of 6 steps of the accelerometer is obtained. The vibration frequency of each step is shown in Table 3. The vibration model that corresponds to the frequency of each step is shown in Fig. 9.

According to the simulation results, the sensitivity direction of the accelerometer is the Z axis. In addition, the second working frequency is larger than the first one. The coupling vibration can be effectively avoided, the sensitivity of the sensor is more stable and the sensitivity is higher.

As shown in Fig. 10 (b), (c), the second and third-order mode vibration directions are twisted along the X and Y axis directions to reduce the risk of electrostatic adsorption.

To reduce the loss of the signal due to lateral motion, the design scheme of the metal plate is proposed with the upper and lower glass larger than the mass area and the sensitivity of the accelerometer is effectively improved.

III. PROCESS

According to the structural characteristics, the process flow can be divided into two parts: (1) silicon plate preparation and (2) glass plate preparation. The overall processing flow is shown in Fig. 11 [18]–[21].

A. Preparation. Prepare the Si wafer.

B. Deposition of Si3N4. Sputter Si3N4 on both sides of the wafer.

C. Inductively coupled plasma (ICP). On both sides of the wafer, etch the Si3N4.

D. ICP. On both sides of the wafer, etch the Si and prepare the damping clearance.

E. Oxidation. Oxidize both sides of the wafer.

F-G. Deep reactive ion etching (DRIE). Etch both sides of the wafer and release the cantilevers.

H. Preparation. Prepare the glass wafer.

I. Through-hole process. Laser drill the upper glass plate.

J. Electroplating. Electroplate metal Cu on top of the glass.

K-L. Sputtering of the metal wire. Sputter Al wire on the bottom of the upper glass, realizing interconnects on both sides of the glass.

M. Sputtering of the metal wire. Sputter Al wire beneath the glass.

N. Oxidation. Oxidize the metal wire to avoid contact between the silicon and glass beneath.

O. Bonding. Achieve the "sandwich" capacitive accelerometer.

Fig. 12 shows the accelerometer topography under scanning electron microscopy, and Fig. 13 shows the accelerometer topography and the package imaged with a charge-coupled device (CCD) camera.

IV. TESTING

A. STATIC TEST

In this paper, wire bonding is used to realize a connection between the metal pad of the accelerometer and the circuit board to complete the package. The capacitance signal is detected by an Agilent E4990A impedance analyzer, as shown in Fig. 14. The capacitive test results are shown in Table 4.

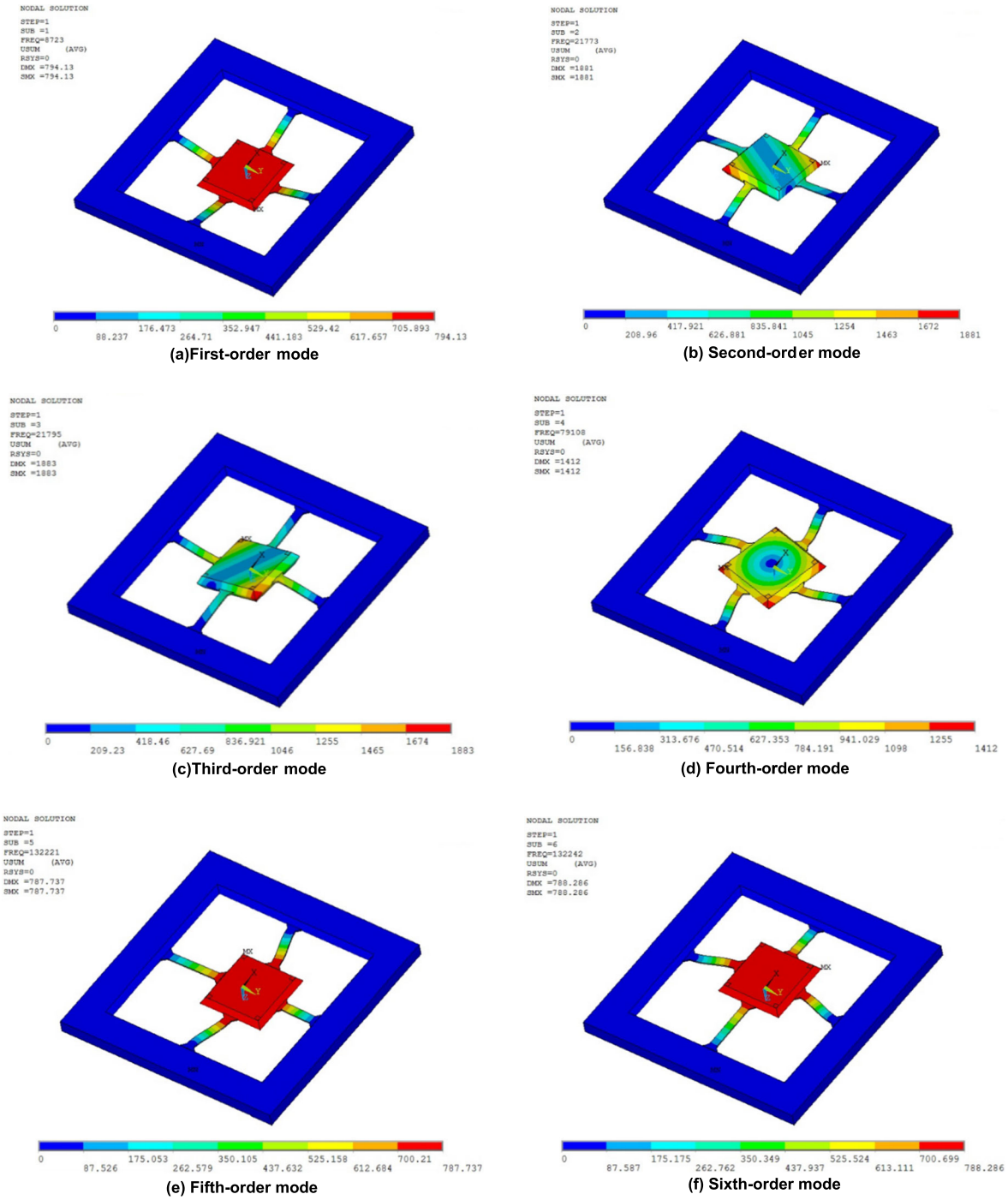

FIGURE 10. The first six modes of the acceleration- sensitive unit.

In this paper, the calculated static capacitance of the accelerometer is $C = \varepsilon A/d = 1.51$ pF. In practice, however, the sensor itself is subjected to acceleration due to gravity. According to the finite element simulation, the stress of the sensor in this situation is 0.12 MPa, and the equivalent displacement is 0.15 μm. Therefore, the theoretical values of the Upper and Lower Capacitances are:

$$C_{UP} = 1.4964 \text{ pF} \quad \text{and } C_{DOWN} = 1.5257 \text{pF}.$$

B. A ± 1 g FLIP TEST OF THE CAPACITIVE ACCELEROMETER

This part carries out a measurement of the upper and lower capacitances by changing the angle of the sensor without an external impact.

The accelerometer is placed at different angles, 0°, 30°, 45°, 60°, 90°, 135°, and 180°, to complete the static capacitance test. The test results are shown in Table 5.

TABLE 4. The static capacitance test results of the device.

Times	Test frequency	Upper electrode		Lower electrode	
		Current (μA)	Capacitance (pF)	Current (μA)	Capacitance (pF)
1	100 k	0.734	1.513	0.83	1.569
2	200 k	1.602	1.505	1.78	1.581
3	300 k	2.812	1.511	2.89	1.573
4	400 k	3.798	1.512	3.99	1.579
5	500 k	4.349	1.513	4.68	1.579

TABLE 5. Flips of the capacitance values at different angles.

	0°	30°	45°	60°	90°	135°	180°
C_{UP} (pF)	1.457	1.460	1.463	1.468	1.472	1.480	1.482
C_{DOWN} (pF)	1.498	1.493	1.490	1.486	1.481	1.475	1.466

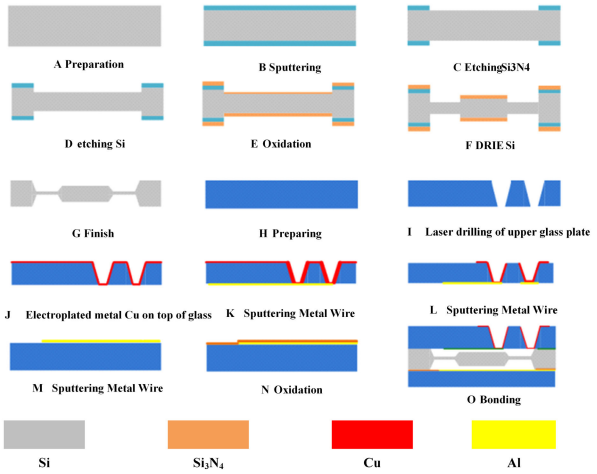

FIGURE 11. Process flow of the capacitive accelerometer.

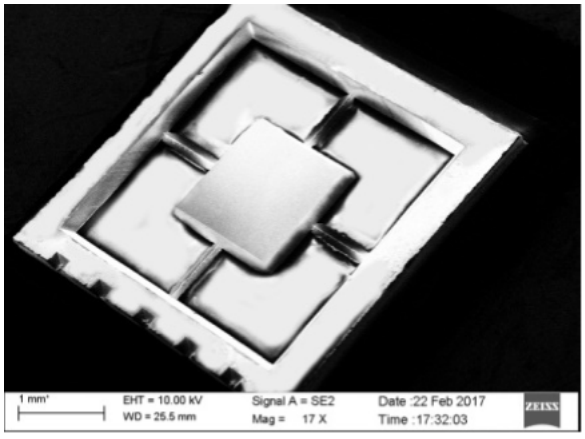

FIGURE 12. Field-emission scanning electron micrograph.

In the theoretical calculation, when the capacitive accelerometer is positioned vertically, the upper and lower capacitance values of the accelerometer should be equal, but due to a deviation in the processing process, there is a difference between the upper and lower capacitances. According to Fig. 15, the upper and lower capacitances are approximately

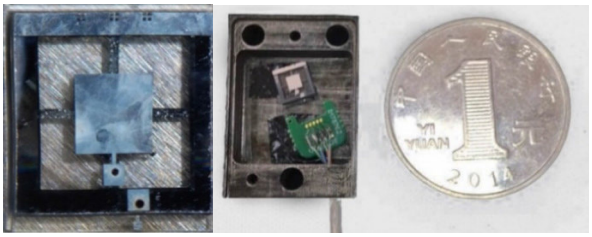

(a) Schematic of the sensor (b) Device package diagram

FIGURE 13. Overall package of the device.

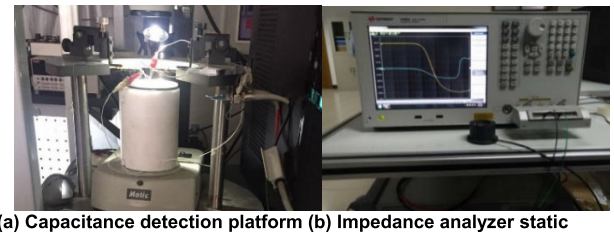

(a) Capacitance detection platform (b) Impedance analyzer static capacitance test

FIGURE 14. Static capacitance test of the device.

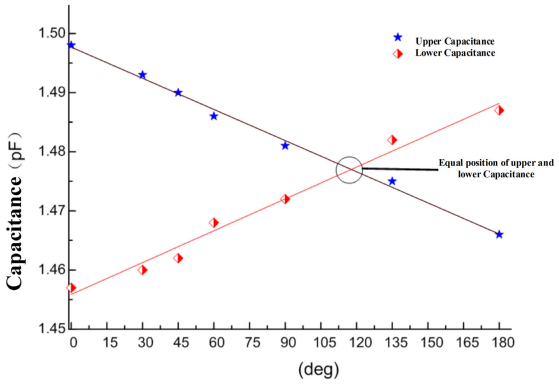

FIGURE 15. Test of the static capacitance values at different angles.

equal when the angle is close to 120°C. By the calculation, the deviation is as follows:

$$\delta_{上} = \frac{|1.472 - 1.51|}{1.51} \times 100\% = 2.51\%,$$

$$\delta_{下} = \frac{|1.481 - 1.51|}{1.51} \times 100\% = 1.92\%.$$

Because the deviation is less than 5%, the structural errors caused by processing flow is negligible and basically meets the test requirements in a low range.

C. DYNAMIC TEST

To verify the anti-overload characteristics of the accelerometer, impact experiments with a Marshall hammer are carried out. The Marshall hammer is a device that is widely used in impact test with its low cost and high availability. The maximum acceleration amplitude can be more than 30,000g, and pulse width is about 90us. The Marshall hammer is mainly composed of a hammer, a runner, a connecting rod, a hammerhead and an iron ingots, and the acceleration sensor is fixed on the hammer by a specific clamp. The sling hammer converts the gravitational potential energy into kinetic energy, which

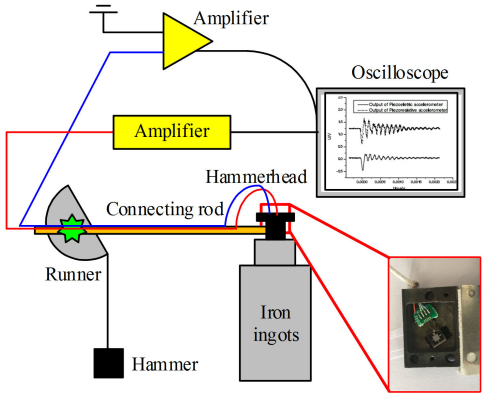

(a) Schematic of Marshall hammer

(b) Testing of sensor by Marshall hammer

FIGURE 16. Marshall hammer calibration device.

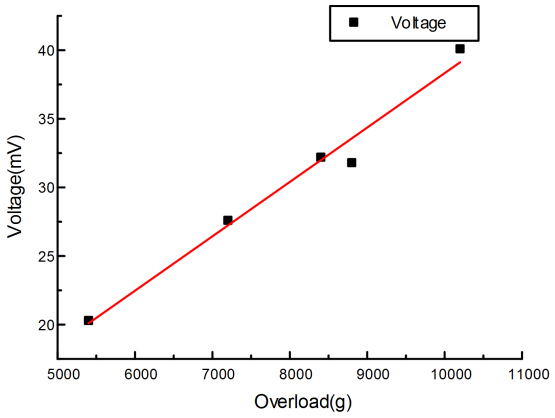

FIGURE 17. Sensor sensitivity fitting curve.

TABLE 6. Overload impact correspondence table.

Standard sensor (V)	Overload (g)	Capacitive accelerometer (V)
0.54	5,400	5.79
0.72	7,200	6.16
0.84	8,400	6.03
1.02	10,200	5.69
1.98	19,800	6.10

TABLE 7. Sensitivity test results of the capacitive accelerometer under different impact environments (applying a Z axis load).

Overload	5,400g	7,200g	8,400g	10,200g
Sensitivity (μV/g)	3.74	3.79	3.84	3.93

drives the runner, the connecting rod and the hammerhead to rotate, so that the hammerhead hits on the iron ingots and generates an impact overload. Fig.16. shows Marshall Hammer device schematic. The sensitivity of the accelerometer is calibrated by comparing the capacitive accelerometer with a standard sensor. In the impact experiments, a 988 piezoelectric accelerometer is used as the standard sensor, and the sensitivity of the sensor is 0.399 pC/g. In this paper, the carrier voltage of the channel from the silicon plate is + 5 V. The channel from the upper and lower glass plates is powered by a + 8 V power supply, and the output of the capacitive accelerometer is sent to an oscilloscope. Different overload impact tests are carried out 6 times with the capacitive accelerometer, and the testing results are shown in Table 6. Under an overload, the output voltage is fitted with the acceleration, and the fitting line is obtained, as shown in Fig. 18. The sensitivity of the capacitive accelerometer along the Z axis at different g values is obtained by a calculation, as shown in Table 7.

Through the tests, it is found that the output voltages are similar under different overload conditions. The result is that under a high-overload environment, the capacitance changes of the accelerometer are equal, and the sensor does not fail; thus, the anti-overload characteristics of the accelerometer are verified.

The data are processed according to the output voltage of the capacitive accelerometer. In this paper, an amplification circuit with a magnification of 187 times is used to convert the capacitive signal into the voltage signal of the capacitive acceleration sensor, and the data of the sensor output voltage and the impact acceleration are simulated. The output sensitivities of the measured capacitive accelerometer along the Z axis under different g values are shown in Table 7.

Through the Marshall hammer impact tests, the sensor exhibits stable output under overload environments of 5,400g, 7,200g, 8,400g, 8,800g and 10,200g, and the output sensitivity is fitted to be 3.96 μV/g.

V. CONCLUSION

A novel capacitive accelerometer with anti-overload characteristics and low range has been presented in this paper. The design, employing a beam-mass structure which is packaged in a sandwich form. The reliability in high impact environments and efficiency in low ranges are achieved by a series of simulations and optimizations. Static and dynamic tests were performed, the results indicate that the capacitance error is less than 5%, the sensitivity of the prototype is 3.96 μV/g which is stable under high impact environments.

REFERENCES

[1] J. Beitia, P. Loisel, and C. Fell, "Miniature accelerometer for high-dynamic, precision guided systems," in *Proc. IEEE Int. Symp. Inertial Sensors Syst. (INERTIAL)*, Kauai, Hawaii, USA, Mar. 2017, pp. 35–38.

[2] J. LöTters, W. Olthuis, P. Veltink, and P. Bergveld, "Design, realization and characterization of a symmetrical triaxial capacitive accelerometer for medical applications," *Sens. Actuators A, Phys.*, vol. 61, nos. 1–3, pp. 303–308, Jun. 1997, doi: 10.1016/s0924-4247(97)80279-8.

[3] H.-H. Hsu, W.-J. Peng, T. K. Shih, T.-W. Pai, and K. L. Man, "Smartphone indoor localization with accelerometer and gyroscope," in *Proc. 17th Int. Conf. Netw.-Based Inf. Syst.*, Sep. 2014, pp. 465–469.

[4] G.-S. Lee, S.-H. Ahn, S.-D. Shon, and S.-J. Lee, "A study on the accelerometer for the acceleration and inclination estimation of structures using double-FBG optical sensors," *J. Korean Assoc. Spatial Struct.*, vol. 16, no. 1, pp. 85–94, Mar. 2016, doi: 10.9712/kass.2016.16.1.085.

[5] A. Aydemir, Y. Terzioglu, and T. Akin, "A new design and a fabrication approach to realize a high performance three axes capacitive MEMS accelerometer," *Sens. Actuators A, Phys.*, vol. 244, pp. 324–333, Jun. 2016, doi: 10.1016/j.sna.2016.04.007.

[6] D. Yamane, T. Matsushima, T. Konishi, H. Toshiyoshi, K. Masu, and K. Machida, "A dual-axis MEMS capacitive inertial sensor with high-density proof mass," *Microsyst Technol*, vol. 22, no. 3, pp. 459–464, Mar. 2016, doi: 10.1007/s00542-015-2539-y.

[7] X. Zhou, L. Che, S. Liang, Y. Lin, X. Li, and Y. Wang, "Design and fabrication of a MEMS capacitive accelerometer with fully symmetrical double-sided H-shaped beam structure," *Microelectron. Eng.*, vol. 131, pp. 51–57, Jan. 2015, doi: 10.1016/j.mee.2014.10.005.

[8] Y. Zhang, "A capacitive micro-accelerometer based on LTCC laminates," *Chin. J. Sens. Actuators*, vol. 29, pp. 467–473, 2016, doi: 10.3969/j.issn.1004-1699.2016.04.001.

[9] M. Keshavarzi and J. Yavand Hasani, "Design and optimization of fully differential capacitive MEMS accelerometer based on surface micromachining," *Microsyst. Technol.*, vol. 25, no. 4, pp. 1369–1377, Apr. 2019, doi: 10.1007/s00542-018-4187-5.

[10] C.-P. Hsu, M.-C. Yip, and W. Fang, "Implementation of a gap-closing differential capacitive sensingZ-axis accelerometer on an SOI wafer," *J. Micromech. Microeng.*, vol. 19, no. 7, Jul. 2009, Art. no. 075006, doi: 10.1088/0960-1317/19/7/075006.

[11] Q. Hu, C. Gao, Y. Hao, Y. Zhang, and G. Yang, "Low cross-axis sensitivity micro-gravity microelectromechanical system sandwich capacitance accelerometer," *Micro Nano Lett.*, vol. 6, no. 7, p. 510, 2011, doi: 10.1049/mnl.2011.0137.

[12] M. Amereh, M. Aghdam, and M. Golkaram, "Design and modeling of a novel translational and angular micro-electromechanical accelerometer," *Aerosp. Sci. Technol.*, vol. 50, pp. 15–24, Mar. 2016, doi: 10.1016/j.ast.2015.12.010.

[13] M.-H. Bao, *Micro Mechanical Transducers Pressure Sensors, Accelerometers and Gyroscopes*, 1st ed. Amsterdam, The Netherlands: Elsevier, 2000.

[14] K. Biswas, S. Sen, and P. K. Dutta, "MEMS capacitive accelerometers," *Sensor Lett.*, vol. 5, no. 3, pp. 471–484, Sep. 2007, doi: 10.1166/sl.2007.201.

[15] M. Benmessaoud and M. M. Nasreddine, "Optimization of MEMS capacitive accelerometer," *Microsyst. Technol.*, vol. 19, no. 5, pp. 713–720, May 2013, doi: 10.1007/s00542-013-1741-z.

[16] C.-M. Sun, C. Wang, and W. Fang, "On the sensitivity improvement of CMOS capacitive accelerometer," *Sens. Actuators A, Phys.*, vol. 141, no. 2, pp. 347–352, Feb. 2008, doi: 10.1016/j.sna.2007.10.026.

[17] J. He, J. Xie, X. He, L. Du, and W. Zhou, "Analytical study and compensation for temperature drifts of a bulk silicon MEMS capacitive accelerometer," *Sens. Actuators A, Phys.*, vol. 239, pp. 174–184, Mar. 2016, doi: 10.1016/j.sna.2016.01.026.

[18] M. Mehran and S. Mohajerzadeh, "High sensitivity nanostructure incorporated interdigital silicon based capacitive accelerometer," *Microelectron. J.*, vol. 46, no. 2, pp. 166–173, Feb. 2015, doi: 10.1016/j.mejo.2014.10.008.

[19] Y. Fan, P. Han, P. Liang, Y. Xing, Z. Ye, and S. Hu, "Differences in etching characteristics of TMAH and KOH on preparing inverted pyramids for silicon solar cells," *Appl. Surf. Sci.*, vol. 264, pp. 761–766, Jan. 2013, doi: 10.1016/j.apsusc.2012.10.117.

[20] L. Wang, Y. He, Z. Zhan, L. Yu, H. Wang, and D. Chen, "A novel sacrificial-layer process based on anodic bonding and its application in an accelerometer," *AIP Adv.*, vol. 5, no. 4, Apr. 2015, Art. no. 041323, doi: 10.1063/1.4907930.

[21] G. Barillaro, "Porous silicon micromachining technology," in *Handbook of Porous Silicon*, L. Canham, Ed. Cham, Switzerland: Springer, 2014. [Online]. Available: https://link.springer.com/referenceworkentry/10.1007%2F978-3-319-05744-6_79#citeas

YUNBO SHI received the B.S. and M.S. degrees from the North University of China, China, in 1995 and 2003, respectively, and the Ph.D. degree from the Beijing Institute of Technology, China, in 2014. He is currently a Professor with the North University of China. His research interest is in the fields of measurement, semiconductor materials, and devices.

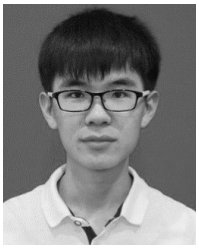

YANLIN WANG is currently pursuing the master's degree with the School of Instrument and Electronics, North University of China. He is currently a Researcher with the Science and Technology on Electronic Test and Measurement Laboratory, North University of China. His research interest is in the fields of packaging and testing of MEMS devices.

HENGZHEN FENG received the M.S. degree with the North University of China, in 2017. He is currently pursuing the Ph.D. degree with the Beijing Institute of Technology. His research interest is in the fields of structural design and processing technology of MEMS devices.

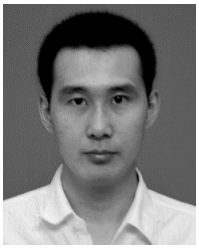

RUI ZHAO received the B.S. degree in microelectronics and the M.E. degree in micro-electronics and solid state electronics from the North University of China, Taiyuan, China, in 2009 and 2012, respectively, and the Ph.D. degree in microelectronics and solid state electronics from the Institute of Microelectronics, Peking University, Beijing, China, in 2016. He is currently working as a Junior Research Fellow with the Science and Technology on Electronic Test and Measurement Laboratory, School of Instrument and Electronics, and the Ministry of Education Key Laboratory Instrumentation Science and Dymanic Measurement, North University of China. His current research interest includes design and fabrication of MEMS/NEMS/MOEMS inertial sensors. He is also working in the field of development of MEMS/NEMS bio/chemical sensors, the self-assembly of nanomaterials, and the development of biosensor devices based on plasmonics.

HUILIANG CAO (Member, IEEE) received the Ph.D. degree in instrument science and technology from Southeast University, Nanjing, China, in 2014. From 2011 to 2012, he studied as a Research Ph.D. Student with the School of Electrical and Computer Engineering, Georgia Institute of Technology, Atlanta, GA, USA. He is one of the Top Young Academic Leaders of Higher Learning Institutions of Shanxi and Young Academic Leaders of North University of China. He is currently a Postgraduate Tutor and an Associate Professor with the School of Instrument and Electronics, North University of China, Taiyuan, China. His research interest includes the areas of MEMS inertial devices.

JUN LIU received the Ph.D. degree from the Beijing Institute of Technology, Beijing, China, in 2001. From 2001 to 2005, he was a Postdoctoral Researcher with Peking University. He is currently a Distinguished Professor with the North University of China, Taiyuan, China. His current research interests include intelligent instrument, micro inertia devices, and micro electromechanical systems devices.